

# Mechanism Design and Motion Analysis of Heavy-Load Transfer Robot with Parallel Four-Bar Mechanism

ZHANG Jing<sup>1\*</sup>, WANG Dongbao<sup>1</sup>, WU Guangping<sup>2</sup>,  
GUO Hongwei<sup>3</sup>, LIU Rongqiang<sup>3</sup>

1. College of Mechanical and Vehicle Engineering, Taiyuan University of Technology, Taiyuan 030024, P. R. China;
2. School of Electronic Information and Electrical Engineering, Shanghai Jiao Tong University, Shanghai 200240, P. R. China;
3. State Key Laboratory of Robotics and System, Harbin Institute of Technology, Harbin 150001, P. R. China

(Received 24 July 2021; revised 13 September 2021; accepted 15 May 2022)

**Abstract:** Heavy-load transfer robots are widely used in automobile production and machinery manufacturing to improve production efficiency. In order to meet the needs of large billet transfer, a 4-DOF transfer robot is designed in this paper, which consists of parallel four-bar mechanisms. The Jacobian matrix referring to the mapping matrix from the joint velocity to the operating space velocity of the transfer robot can be solved by the differential-vector method. The mean value of the Jacobian matrix condition number in the workspace is used as the global performance index of the robot velocity and the optimization goal. The constraint condition is established based on the actual working condition. Then the linkage length optimization is carried out to decrease the length of the linkage and to increase the global performance index of velocity. The total length of robot rods is reduced by 6.12%. The global performance index of velocity is improved by 45.15%. Taking the optimized rod length as the mechanism parameter, the distribution of the motion space of the transfer robot is obtained. Finally, the results show that the proposed method for establishing the Jacobian matrix of the lower-mobility robot and for the optimization of the rods based on the velocity global performance index is accurate and effective. The workspace distribution of the robot meets the design requirements.

**Key words:** parameter optimization; motion analysis; mechanism design; transfer robot; heavy-load

**CLC number:** TP242.2      **Document code:** A      **Article ID:** 1005-1120(2022)05-0606-13

## 0 Introduction

With the development of automation technology, industrial robots have gradually replaced traditional manpower in simple and repetitive tasks. In addition, because of the great application prospect of industrial robots, this is known as one of the three pillars of industrial automation<sup>[1]</sup>. As a kind of industrial robot, heavy-load transfer robots have been widely used in various industries, such as automobile production, machinery manufacturing, palletizing logistics, especially in the harsh environment not suitable for human work<sup>[2-3]</sup>.

In the 1950s, the American Devol Company

designed and developed the earliest industrial robot. The robot needs to input a predetermined motion path in advance. It is also known as a teach-repeat industrial robot. The motion accuracy and response speed are relatively low due to adopting open-loop control. By the end of the 1970s, these characteristics of industrial robots represented by PUMA robots had been improved. Since then, the countries around the world have carried out structural improvements and performance optimization of transfer robots with the goal of high stability, high reliability, and low weight ratio. American Par Systems Company introduced a Cartesian coordinate in-

\*Corresponding author, E-mail address: free1985216@163.com.

**How to cite this article:** ZHANG Jing, WANG Dongbao, WU Guangping, et al. Mechanism design and motion analysis of heavy-load transfer robot with parallel four-bar mechanism[J]. Transactions of Nanjing University of Aeronautics and Astronautics, 2022, 39(5): 606-618.

<http://dx.doi.org/10.16356/j.1005-1120.2022.05.009>

dustrial robot. Japan developed SCARA robotic arm that contains both slider joints and revolute joints. YASKAWA Company used the parallel four-bar mechanism for mechanical arm structure design, and developed a new type of robot with low-weight and high-load. Foreign industrial robots are mainly light-load robots, which are mainly used in fast-response working environments and small spaces. For example, the ABB-IRB6640 robot with a transfer speed of up to 3.3 m/s can be loaded with a payload of 200 kg. In China, the research on industrial robots started late. After more than half a century of development, research institutions and robot companies of China have made many achievements. For example, Harbin Boshi Robot Company has developed a professional robot with a payload of 300 kg. Siasun Robotics developed an industrial robot with independent intellectual property rights and with a payload of 120 kg. Harbin Institute of Technology and Shanghai University independently developed transfer robots with independent intellectual property rights. At present, articulated robots, as the main robots, have the advantages of large workspace and high flexibility. However, the positional accuracy of the industrial robots under high-speed and heavy-load conditions has reduced because of the complexity of rotary joint structures. Therefore, it is of great significance to design and develop a new type of heavy-load transfer robot.

Yang et al.<sup>[4]</sup> proposed a detailed scheme design for heavy-load transfer robots based on the parallel equations and transfer constraint conditions. Fukui et al.<sup>[5]</sup> put forward a hoisting mobile robot Han-Grawler, which has high mobility and can freely choose and adjust the route. The robot can achieve linear translational motion at a speed of 0.1 m/s and rotational motion at a speed of 8.5 °/s by installing a mechanical restraint suspension mechanism. Zhu et al.<sup>[6]</sup> used the D-H method to establish the kinematics model of the 150 kg heavy-load robot independently. The singular posture of the robot was developed and analyzed based on the inverse kinematics analysis. Ma et al.<sup>[7]</sup> designed a simplified 3-DOF parallel robot based on the FANUC transfer manipulator. The size of the mechanism was optimized by

using the velocity global performance index and the acceleration global performance index. Rioux et al.<sup>[8]</sup> aimed at the navigation problem of the transfer robot when moving large heavy objects. They proposed a system solution from the incremental construction of the environment map and the calculation of collision-free trajectories to the execution of these trajectories. The solution significantly increased the transfer payload of the robot when the main hardware of the robot was not changed. According to the structural characteristics of heavy-duty transport robots, Yang et al.<sup>[9]</sup> used ADAMS to obtain the relationship between error fluctuations and the movement of key parts of the robot by conducting kinematics simulation. The peak torque characteristics of key parts were analyzed to guide the selection of the drive motor. Wang et al.<sup>[10]</sup> analyzed the velocity global performance index of a 5-DOF parallel mechanism based on the Jacobian matrix to obtain the influence of the size of movable platform and fixed platform on mechanism performance, and the dimension of the mechanism with better velocity performance.

In order to improve the control accuracy of the palletizing robot operation, Xiong et al.<sup>[11]</sup> took ABB-IRB660 palletizing robot as the research object, and carried out workspace calculation and trajectory planning to achieve the optimal motion time under the premise of considering the boundary conditions. Hawley et al.<sup>[12]</sup> proposed a model-based motion controller to realize stable motion control when pushing and transporting heavy objects. The effectiveness of this control strategy was verified by NAO transfer robot experiments. Liu et al.<sup>[13]</sup> proposed a geometric kinematics solution for the 4-DOF parallelogram palletizing robot. Compared with the D-H method, this algorithm has the characteristics of simple computation and convenient real-time control, but it is only suitable for specific forms of robots.

Aiming at an existing heavy-load palletizing robot, Wei et al.<sup>[14]</sup> constructed a motion equation to analyze the kinematics characteristics. The mass of the structure was optimized by using the response surface method and the topology method. At present, a large number of domestic heavy-load transfer

robots rely on imports<sup>[15-17]</sup>. The internationally renowned heavy-load robot manufacturers occupy more than 80% of China's market share<sup>[3]</sup>. The design schemes of the heavy-load robot were carried out by conducting kinematic analysis, robot design optimization and motion control according to the actual requirements of the robot to realize general transferring or special scenarios application.

Therefore, to carry out the mechanism design and kinematics analysis of heavy-load transfer robots, it is necessary to decrease the driving source or motion coupling constraint scheme by taking actual workspace as a constraint. According to the technical parameter requirements of the robot, based on principles of high rigidity, high strength and simple control, this paper proposes a configuration scheme of a material transfer robot with multi-parallel four-bar mechanisms and carries out the overall mechanism design. The forward kinematic problem of the robot is calculated by using the D-H parameter method. The inverse kinematic problem is solved by using the inverse transform method and geometric analytic method. The Jacobian matrix of the robot is obtained by synthesizing the total differential equation method and the vector product method. The op-

timization of the length of the robot rod and the analysis of workspace are carried out.

## 1 Mechanism Design of Heavy-Load Transfer Robot

The overall schematic diagram of the heavy-load transfer robot is shown in Fig.1, including the upper arm, the elbow, the vertical arm, the longitudinal parallel linkage, the transverse parallel linkage, the auxiliary triangle plate, driving linkage of the elbow, supporting linkage of the elbow, the long rod, the short rod, the driving linkage and clamp connecting rod of the linear motion mechanism. The slewing support rotates around the fixed base through the hydraulic motor installed on the slewing support. Since the whole machine rotates around the bottom rotation axis, when the bottom rotation degree of freedom is removed, the mechanism can be converted to a plane mechanism. The degrees of freedom of the robot can be calculated by

$$F = 3 \times (N - 1) - (2P_1 + P_h - P') \quad (1)$$

where  $N$ ,  $P_1$ ,  $P_h$  and  $P'$  are the numbers of components, low pairs, high pairs and redundant constraints, respectively.

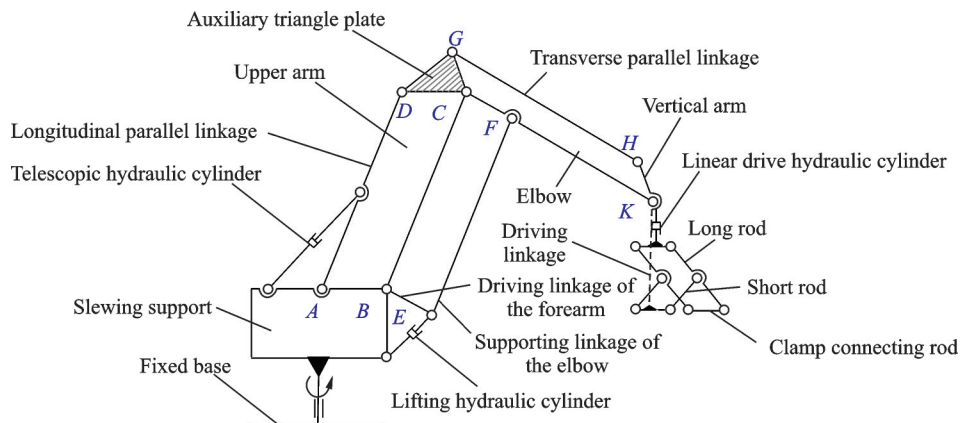


Fig.1 Schematic diagram of the transfer robot

From Fig.1, it can be seen that  $N=19$ ,  $P_1=26$ ,  $P_h=0$  and  $P'=1$ . The degree of freedom of the plane mechanism is 3. Finally, the space rotation degree of freedom is added to the overall degree of freedom of the mechanism. The robot has 4 degrees of freedom.

To improve the capacity of the robot, four par-

allel four-bar mechanisms are used in the robot. The first parallel four-bar mechanism is composed of the upper arm, the longitudinal parallel linkage, the slewing support and bottom edge of the auxiliary triangle plate. The bottom edge of the auxiliary triangle plate is always parallel to the ground during the movement. The auxiliary telescopic hydraulic cylin-

der pushes the robot to achieve horizontal expansion. The second parallel four-bar mechanism is composed of the elbow, the transverse parallel linkage, the upper part of the vertical arm and the right side of the auxiliary triangle plate. The vertical arm always maintains upright during the movement. The third parallel four-bar mechanism is composed of the upper arm, the elbow, the driving link of the elbow and the supporting link of the elbow, which assists the lifting hydraulic cylinder to promote vertical lifting movement of the robot. The hinge point of the short rod and the long rod of the linear motion mechanism is at the middle point of the long rod. The fourth parallel four-bar mechanism is composed of two long rods, the driving linkage and the clamp linkage. The clamp connecting rod keeps horizontal all the time. The driving linkage is equipped with a sliding block, which forms a sliding pair with the guide rail installed on the vertical arm. The linear motion mechanism is driven by the driving hydraulic cylinder installed on the vertical arm.

## 2 D-H Coordinate System and Jacobian Matrix

### 2.1 D-H coordinate system establishment and coordinate transformation

There are many parallelograms in the robot. The kinematic simplification can be conducted<sup>[18]</sup>. According to the characteristics of the parallelogram,  $AD//BC$  and  $EF//BC$ , the rods  $AD$ ,  $BC$ , and  $EF$ , which are shown in Fig.1, are in the same direction at any time. Therefore, rod  $BC$  can be used as the equivalent rod for the upper arm. In the same way, in the parallelogram  $CGHK$ , the rod  $CK$  can be used as the equivalent rod for the elbow. According to the preliminary designed transfer mechanism, the simplified diagram of the transfer robot mechanism marked with the D-H coordinate system is shown in Fig.2. The upper arm length  $l_2$ , the elbow length  $l_3$ , the vertical rod length  $l_4$ , the lengths of the clamping rods lengths  $l_5$  and  $l_6$  are given in Fig.2. The rod parameters of

the robot are shown in Table 1, where  $\theta_i$  is the angle of rotating around the  $Z_{i-1}$ -axis, from  $X_{i-1}$ -axis to  $X_i$ -axis in the D-H coordinate system which is shown in Fig.2.

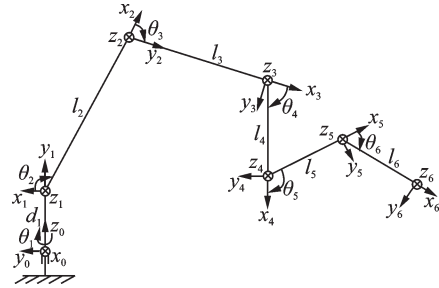


Fig.2 Simplified diagram of transfer robot mechanism

Table 1 Linkage parameters of transfer robot

Joint $i$	$\theta_i/(^\circ)$	$\alpha_i/(^\circ)$	$l_i/\text{mm}$	$d_i/\text{mm}$	Range of variation/ $(^\circ)$
1	$\theta_1$	90	0	$d_1$	-180—180
2	$\theta_2$	0	$l_2$	0	60—150
3	$\theta_3$	0	$l_3$	0	45—135
4	$\theta_4$	0	$l_4$	0	Determined by $\theta_2$ and $\theta_3$
5	$\theta_5$	0	$l_5$	0	-90—-180
6	$\theta_6$	0	$l_5$	0	Determined by $\theta_5$

As shown in Fig.2,  $\theta_4$  is the acute angle between the elbow and the vertical rod. Since the vertical rod remains vertical at all time,  $\theta_4$  is mainly determined by the posture of the elbow. The lengths of the two clamping rods are equal,  $l_5=l_6$ . The horizontal angles of the two rods are equal. According to the geometric parameters of each member of the robot and the relationship of the positions between each other, it can be obtained that

$$\theta_4 = 270^\circ - \theta_2 - \theta_3, \theta_6 = -180^\circ - 2\theta_5 \quad (2)$$

According to the method of establishing the D-H coordinate system and the simplified diagram of the transfer robot, a homogeneous transformation matrix  ${}^{i-1}T_i$  between adjacent coordinate systems  $\sum O_{i-1}$  and  $\sum O_i$  is established.

$${}^{i-1}T_i = \begin{bmatrix} \cos \theta_i & -\cos \alpha_i \sin \theta_i & \sin \alpha_i \sin \theta_i & l_i \cos \theta_i \\ \sin \theta_i & \cos \alpha_i \cos \theta_i & -\sin \alpha_i \cos \theta_i & l_i \sin \theta_i \\ 0 & \sin \alpha_i & \cos \alpha_i & d_i \\ 0 & 0 & 0 & 1 \end{bmatrix} \quad (3)$$

Therefore, the D-H transformation matrix between each rod can be obtained as

$${}^0T_1 = \begin{bmatrix} c_1 & 0 & s_1 & 0 \\ s_1 & 0 & -c_1 & 0 \\ 0 & 1 & 0 & d_1 \\ 0 & 0 & 0 & 1 \end{bmatrix}, {}^1T_2 = \begin{bmatrix} c_2 & -s_2 & 0 & l_2c_2 \\ s_2 & c_2 & 0 & l_2s_2 \\ 0 & 0 & 1 & 0 \\ 0 & 0 & 0 & 1 \end{bmatrix}$$

$${}^2T_3 = \begin{bmatrix} c_3 & -s_3 & 0 & l_3c_3 \\ s_3 & c_3 & 0 & l_3s_3 \\ 0 & 0 & 1 & 0 \\ 0 & 0 & 0 & 1 \end{bmatrix}, {}^3T_4 = \begin{bmatrix} c_4 & -s_4 & 0 & l_4c_4 \\ s_4 & c_4 & 0 & l_4s_4 \\ 0 & 0 & 1 & 0 \\ 0 & 0 & 0 & 1 \end{bmatrix}$$

$${}^4T_5 = \begin{bmatrix} c_5 & -s_5 & 0 & l_5c_5 \\ s_5 & c_5 & 0 & l_5s_5 \\ 0 & 0 & 1 & 0 \\ 0 & 0 & 0 & 1 \end{bmatrix}, {}^5T_6 = \begin{bmatrix} c_6 & -s_6 & 0 & l_5c_6 \\ s_6 & c_6 & 0 & l_5s_6 \\ 0 & 0 & 1 & 0 \\ 0 & 0 & 0 & 1 \end{bmatrix}$$

where  $c_i = \cos \theta_i$ ,  $s_i = \sin \theta_i$ . From Eq.(2),  $\cos(\theta_2 + \theta_3) = -\sin \theta_4$ ,  $\sin(\theta_2 + \theta_3) = -\cos \theta_4$ ,  $\cos(\theta_2 + \theta_3 + \theta_4) = 0$ ,  $\sin(\theta_2 + \theta_3 + \theta_4) = -1$ ,  $\cos(\theta_2 + \theta_3 + \theta_4 + \theta_5) = \sin \theta_5$ ,  $\sin(\theta_2 + \theta_3 + \theta_4 + \theta_5) = -\cos \theta_5$ ,  $\cos(\theta_2 + \theta_3 + \theta_4 + \theta_5 + \theta_6) = \sin \theta_5$ ,  $\sin(\theta_2 + \theta_3 + \theta_4 + \theta_5 + \theta_6) = \cos \theta_5$ .

The transformation matrix  ${}^0T_6$  of the robot end-effector relative to the base coordinate system is expressed as

$${}^0T_6 = {}^0T_1 \cdot {}^1T_2 \cdot {}^2T_3 \cdot {}^3T_4 \cdot {}^4T_5 \cdot {}^5T_6 = \begin{bmatrix} n_x & o_x & a_x & p_x \\ n_y & o_y & a_y & p_y \\ n_z & o_z & a_z & p_z \\ 0 & 0 & 0 & 1 \end{bmatrix} \quad (4)$$

where  $n_x = \cos \theta_1 \sin \theta_5$ ,  $n_y = \sin \theta_1 \sin \theta_5$ ,  $n_z = \cos \theta_5$ ,  $o_x = -\cos \theta_1 \cos \theta_5$ ,  $o_y = -\sin \theta_1 \cos \theta_5$ ,  $o_z = \sin \theta_5$ ,  $a_x = \sin \theta_1$ ,  $a_y = -\cos \theta_1$ ,  $a_z = 0$ ,  $p_x = \cos \theta_1(l_2 \cos \theta_2 - l_3 \sin \theta_4 + 2l_5 \sin \theta_5)$ ,  $p_y = \sin \theta_1(l_2 \cos \theta_2 - l_3 \sin \theta_4 + 2l_5 \sin \theta_5)$ ,  $p_z = l_2 \sin \theta_2 - l_3 \cos \theta_4 - l_4 + d_1$ .

## 2.2 Comparison simulations between the original robot and the equivalent mechanism

In order to verify the equivalence of the mechanism, the three-dimensional model of the mechanism is imported into ADAMS for dynamic comparative analysis. The 3D model of mechanism in ADAMS is shown in Fig.3. The step functions in the driving process are shown in Table 2.

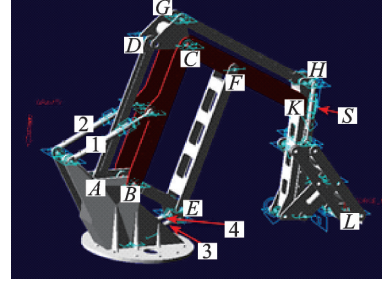


Fig.3 3D model of mechanism in ADAMS

The relationship between the driving displacement and the rotation angle of the rod is shown in Fig.4. The relationship between the displacement of the first drive and angle  $ABC$  of the upper arm is shown in Fig.4(a). The relationship between the displacement of the third drive and angle  $BEF$  is shown in Fig.4(b). Through the diagrams of the relationship between the driving rod and the connecting rod, the displacement of the end  $L$ -point in the  $x$  and  $y$  directions can be clearly observed.

In Fig.5, the  $L$ -point motion trajectory curves at the end of the three-dimensional model and equivalent mechanism are compared. The comparison of changes of the  $L$ -point in the  $x$  direction is shown in Fig.5(a). The comparison of changes of the  $L$ -point

Table 2 Step functions of prismatic pairs

Prismatic pair	Step function
1	$-(33.75 \times \text{time} \times \text{time} \times \text{time} \times \text{time} \times \text{time} + (-168.75) \times \text{time} \times \text{time} \times \text{time} \times \text{time} + 225 \times \text{time} \times \text{time} \times \text{time})$
2	$-(33.75 \times \text{time} \times \text{time} \times \text{time} \times \text{time} \times \text{time} + (-168.75) \times \text{time} \times \text{time} \times \text{time} \times \text{time} + 225 \times \text{time} \times \text{time} \times \text{time})$
3	$112.5 \times \text{time} \times \text{time} \times \text{time} \times \text{time} \times \text{time} + (-562.5) \times \text{time} \times \text{time} \times \text{time} \times \text{time} + 750 \times \text{time} \times \text{time} \times \text{time}$
4	$112.5 \times \text{time} \times \text{time} \times \text{time} \times \text{time} \times \text{time} + (-562.5) \times \text{time} \times \text{time} \times \text{time} \times \text{time} + 750 \times \text{time} \times \text{time} \times \text{time}$
5	$-(75 \times \text{time} \times \text{time} \times \text{time} \times \text{time} \times \text{time} + (-375) \times \text{time} \times \text{time} \times \text{time} \times \text{time} + 500 \times \text{time} \times \text{time} \times \text{time})$

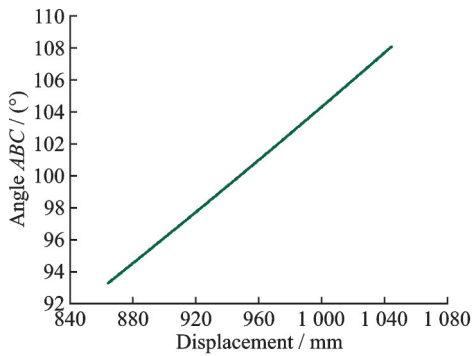
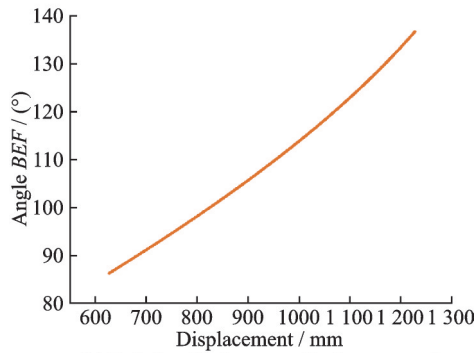
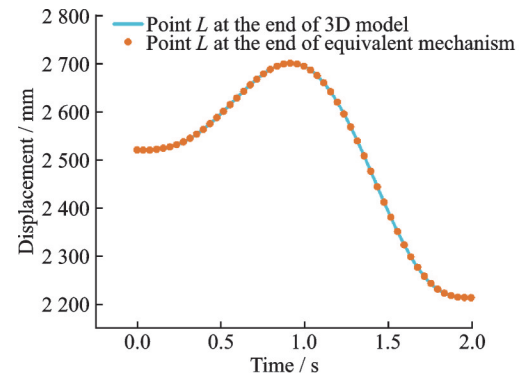
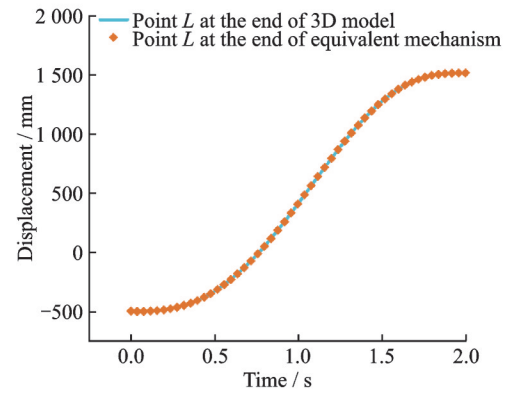
(a) Relationship between displacement of the first drive and angle  $ABC$ (b) Relationship between displacement of the third drive and angle  $BEF$ 

Fig.4 Relationship between the driving displacement and the rotation angle

in the  $y$  direction is shown in Fig.5(b). According to the analysis of the trajectory curve comparison diagram, it can be obtained that the trajectory of the three-dimensional model is consistent with that of the equivalent mechanism. Thus, the correctness of the results is verified, which provides a theoretical basis for the kinematic analysis and size optimization of the mechanism.

### 2.3 Verification of D-H parameters and kinematics equations

In order to verify the correctness of the obtained D-H parameters and kinematics equations, the three-dimensional model of the transfer robot is generated by MATLAB Robotics Toolbox, and the robot control panel is generated at the same time. The control panel can adjust the angles of each joint to make the joint rotate. The robot simulation models are shown in Fig.6. The angles of each joint in the initial state of the robot in Fig.6(a), Fig.6(b) and Fig.6(c) are  $\theta_1=0$ ,  $\theta_2=0$ ,  $\theta_3=0$ ,  $\theta_4=3\pi/2$ ,  $\theta_5=0$ ,  $\theta_6=-\pi$ ,  $\theta_1=\pi/2$ ,  $\theta_2=37.5\pi/18$ ,  $\theta_3=\pi/2$ ,

(a) Comparison of changes of  $L$ -point in the  $x$  direction(b) Comparison of changes of  $L$ -point in the  $y$  directionFig.5 Comparison of  $L$ -point trajectory curves of 3D model and equivalent mechanism

$\theta_4=142.5\pi/18$ ,  $\theta_5=-\pi/2$ ,  $\theta_6=0$  and  $\theta_1=82.5\pi/18$ ,  $\theta_2=135\pi/18$ ,  $\theta_3=\pi/2$ ,  $\theta_4=\pi/4$ ,  $\theta_5=-113\pi/18$ ,  $\theta_6=46\pi/18$ , respectively.

These special values are brought into transformation matrix  ${}^0T_6$  for verification. Let  $d_1=179$  mm,  $l_2=172$  mm,  $l_3=658$  mm,  $l_4=170$  mm,  $l_5=85$  mm, the position coordinates of the end effector are consistent with the values obtained from the 3D model generated in MATLAB. Thus, the correctness of the results is verified, which provides a theoretical basis for the workspace analysis of the mechanism and the solution of the Jacobian matrix.

### 3 Jacobian Matrix Solution

The Jacobian matrix refers to the mapping matrix from the joint velocity to the operating space velocity, which satisfies

$$\mathbf{V} = \mathbf{J}\dot{\boldsymbol{\theta}} \quad (5)$$

where  $\mathbf{V}$  is the operating space velocity,  $\dot{\boldsymbol{\theta}}$  the joint velocity and  $\mathbf{J}$  the Jacobian matrix of the robot.

For a robot with  $n$  joints, its Jacobian matrix is

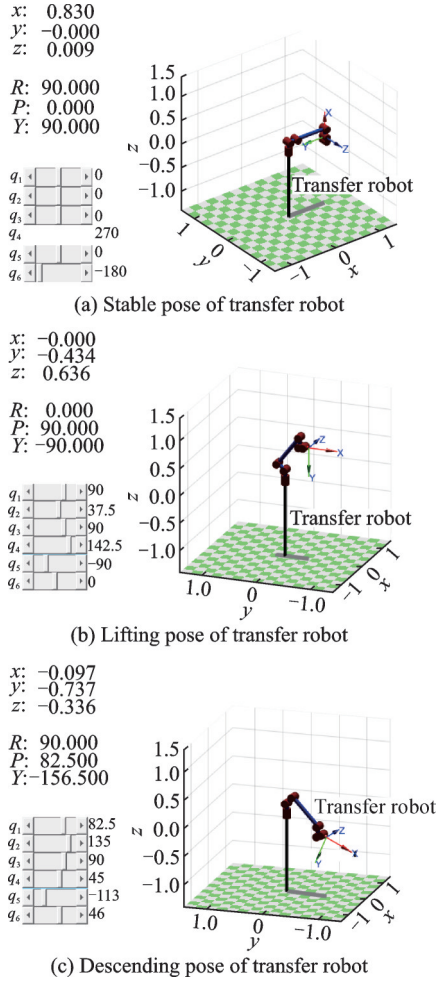


Fig.6 Robot simulation models

a  $6 \times n$ -order matrix. The first three rows represent the transfer ratio of the operator's linear velocity  $v$ . The last three rows represent the transfer ratio of the operator's angular velocity. Each column represents the corresponding joint velocity  $\dot{\theta}_i$  to the transfer ratio of the operator's linear velocity and angular velocity. The Jacobian matrix can be divided as

$$V = \begin{bmatrix} v \\ \omega \end{bmatrix} = \begin{bmatrix} J_1 \\ J_a \end{bmatrix} \dot{\theta} \quad (6)$$

where  $J_1$  is the mapping matrix of joint linear velocity to Cartesian space velocity and  $J_a$  the mapping matrix of joint angular velocity to Cartesian space velocity.

In order to solve the Jacobian matrix, the total differential method and the vector method are combined, which can avoid a large number of matrix operations and matrix inversion operations when compared to the total differential method or the vector method, respectively<sup>[19]</sup>. Therefore, the mapping

matrix  $J_1$  is solved by using the total differentiation method. The mapping matrix  $J_a$  is solved by using the vector method.

### 3.1 Jacobian matrix $J_1$ solution based on the total differential method

The position of the robot end manipulator relative to the robot base coordinate system is expressed as  ${}^0P_6$ , shown as

$${}^0P_6 = \begin{bmatrix} P_x \\ P_y \\ P_z \end{bmatrix} = \begin{bmatrix} f_x(\theta_1, \theta_2, \theta_4, \theta_5) \\ f_y(\theta_1, \theta_2, \theta_4, \theta_5) \\ f_z(\theta_1, \theta_2, \theta_4, \theta_5) \end{bmatrix} \quad (7)$$

According to the definition of the Jacobian matrix, the mapping from the velocity of the end operator to the joint velocity can be got by solving total differential  ${}^0P_6$ , shown as

$$J_1 = \begin{bmatrix} \frac{\partial P_x}{\partial \theta_1} & \frac{\partial P_x}{\partial \theta_2} & \frac{\partial P_x}{\partial \theta_4} & \frac{\partial P_x}{\partial \theta_5} \\ \frac{\partial P_y}{\partial \theta_1} & \frac{\partial P_y}{\partial \theta_2} & \frac{\partial P_y}{\partial \theta_4} & \frac{\partial P_y}{\partial \theta_5} \\ \frac{\partial P_z}{\partial \theta_1} & \frac{\partial P_z}{\partial \theta_2} & \frac{\partial P_z}{\partial \theta_4} & \frac{\partial P_z}{\partial \theta_5} \end{bmatrix} \quad (8)$$

where  $\frac{\partial P_x}{\partial \theta_1} = J_{11} = -l_2 s_1 c_2 + l_3 s_1 s_4 - 2l_5 s_1 s_5$ ,  $\frac{\partial P_x}{\partial \theta_2} =$

$$J_{12} = -l_2 c_1 s_2, \quad \frac{\partial P_x}{\partial \theta_3} = J_{13} = -l_3 c_1 c_4, \quad \frac{\partial P_x}{\partial \theta_4} = J_{14} = 2l_5 c_1 c_5,$$

$$\frac{\partial P_y}{\partial \theta_1} = J_{21} = l_2 c_1 c_2 - l_3 c_1 s_4 + 2l_5 c_1 s_5, \quad \frac{\partial P_y}{\partial \theta_2} = J_{22} =$$

$$-l_2 s_1 s_2, \quad \frac{\partial P_y}{\partial \theta_3} = J_{23} = -l_3 s_1 c_4, \quad \frac{\partial P_y}{\partial \theta_4} = J_{24} = 2l_5 s_1 c_5,$$

$$\frac{\partial P_z}{\partial \theta_1} = J_{31} = 0, \quad \frac{\partial P_z}{\partial \theta_2} = J_{32} = l_2 c_2, \quad \frac{\partial P_z}{\partial \theta_3} = J_{33} = l_3 s_4,$$

$$\frac{\partial P_z}{\partial \theta_4} = J_{34} = 0.$$

### 3.2 Jacobian matrix $J_a$ solution based on the vector method

The movement of each joint of the robot has an impact on the velocity of the robot's end manipulator. Based on the relationship between the joint velocity and the end velocity, velocity  $\omega_i$  at the end of the robot caused by the revolute joint satisfies

$$\omega_i = Z_{i-1} \dot{\theta}_i \quad (9)$$

Then the angular velocity of the robot end satisfies

$$\omega = \sum_{i=1}^6 Z_{i-1} \dot{\theta}_i \quad (10)$$

where  $Z_i$  is the  $Z$  axis of the robot coordinate system  $\sum O_i$ . The mapping from the end angular velocity of the robot to the joint angular velocity is expressed as

$$J_a = [{}^0Z_0 \quad {}^0Z_1 \quad {}^0Z_2 \quad {}^0Z_3 \quad {}^0Z_4 \quad {}^0Z_5] \quad (11)$$

where  ${}^0Z_i$  represents the coordinate of the  $Z$  axis of the coordinate system  $\sum O_i$ , which is relative to the base coordinate system. That is to say, the column vector is composed of the third column elements of  ${}^0T_i$ . Therefore

$${}^0Z_0 = \begin{bmatrix} 0 \\ 0 \\ 1 \end{bmatrix}, {}^0Z_1 = \begin{bmatrix} s_1 \\ -c_1 \\ 0 \end{bmatrix}, {}^0Z_3 = \begin{bmatrix} s_1 \\ -c_1 \\ 0 \end{bmatrix},$$

$${}^0Z_4 = \begin{bmatrix} s_1 \\ -c_1 \\ 0 \end{bmatrix}, {}^0Z_5 = \begin{bmatrix} s_1 \\ -c_1 \\ 0 \end{bmatrix}$$

Deduced from Eq.(6), the operator's angular velocity can be given as

$$J_{6 \times 4} = \begin{bmatrix} -l_2s_1c_2 + l_3s_1s_4 - 2l_5s_1s_5 & -l_2c_1s_2 & -l_3c_1c_4 & 2l_5c_1c_5 \\ -l_2c_1c_2 + l_3c_1s_4 - 2l_5c_1s_5 & -l_2s_1s_2 & -l_3s_1c_4 & 2l_5s_1c_5 \\ 0 & l_2c_2 & l_3s_4 & 0 \\ 0 & 0 & 0 & -s_1 \\ 0 & 0 & 0 & c_1 \\ 1 & 0 & 0 & 0 \end{bmatrix} \quad (16)$$

Eq.(2) shows that the number of independent joint angles of the transfer robot is 4, which belongs to the robot with few degrees of freedom. The Jacobian matrix obtained by Eq.(16) is a rectangular matrix with 6 rows and 4 columns. This kind of Jacobian matrix cannot perform inverse matrix operation. This brings troubles to robot singularity analysis and robot control. For the robot proposed in this paper, the linearly independent velocity in Cartesian space is determined. By recombining the mapping coefficients in the Jacobian matrix corresponding to the linearly independent velocity, the square Jacobian matrix of the robot with few degrees of freedom can be obtained.

Since the row vectors in the first, second, and

$$J_{4 \times 4} = \begin{bmatrix} -l_2s_1c_2 + l_3s_1s_4 - 2l_5s_1s_5 & -l_2c_1s_2 & l_3c_1c_4 & 2l_5c_1c_5 \\ 0 & l_2c_2 & l_3s_4 & 0 \\ 0 & 0 & 0 & c_1 \\ 1 & 0 & 0 & 0 \end{bmatrix} \quad (18)$$

$$\begin{bmatrix} \omega_x \\ \omega_y \\ \omega_z \end{bmatrix} = \begin{bmatrix} 0 & s_1 & s_1 & s_1 & s_1 & s_1 \\ 0 & -c_1 & -c_1 & -c_1 & -c_1 & -c_1 \\ 1 & 0 & 0 & 0 & 0 & 0 \end{bmatrix} \begin{bmatrix} \dot{\theta}_1 \\ \dot{\theta}_2 \\ \dot{\theta}_3 \\ \dot{\theta}_4 \\ \dot{\theta}_5 \\ \dot{\theta}_6 \end{bmatrix} \quad (12)$$

The differential of Eq.(2) can be expressed as

$$\dot{\theta}_4 = -\dot{\theta}_2 - \dot{\theta}_3, \dot{\theta}_6 = -2\dot{\theta}_5 \quad (13)$$

Then Eq.(12) can be simplified as

$$\begin{bmatrix} \omega_x \\ \omega_y \\ \omega_z \end{bmatrix} = \begin{bmatrix} 0 & 0 & 0 & -s_1 \\ 0 & 0 & 0 & c_1 \\ 1 & 0 & 0 & 0 \end{bmatrix} \begin{bmatrix} \dot{\theta}_1 \\ \dot{\theta}_2 \\ \dot{\theta}_4 \\ \dot{\theta}_5 \end{bmatrix} \quad (14)$$

Therefore,  $J_a$  can be expressed as

$$J_a = \begin{bmatrix} 0 & 0 & 0 & -s_1 \\ 0 & 0 & 0 & c_1 \\ 1 & 0 & 0 & 0 \end{bmatrix} \quad (15)$$

Based on Eqs.(8) and (15), the Jacobian matrix of the transfer robot can be given as

sixth rows of Eq.(16) are linear correlation. The vectors in the fourth and fifth rows are linear correlations. There is a set of constants that are not all zeros. So

$$\begin{cases} J(1, :) + k_2J(2, :) + k_6J(6, :) = 0 \\ k_4J(4, :) + k_5J(5, :) = 0 \end{cases} \quad (17)$$

where  $J(i, :)$  is the  $i$ th row vector of the Jacobian matrix of the robot. Choosing one velocity component from  $(v_x, v_y, \omega_z)$  and  $(\omega_x, \omega_y)$  as the subordinate component<sup>[16]</sup>, the remaining four components can be used as independent velocity components. There are 6 possible combinations. Taking  $(v_y, \omega_y)$  as the subordinate velocity component, a  $4 \times 4$  Jacobian matrix with few degrees of freedom can be obtained as

## 4 Size Optimization Based on Velocity Global Performance Index

### 4.1 Design variables and constraints

The simplified structure of the transfer robot is shown in Fig.7.

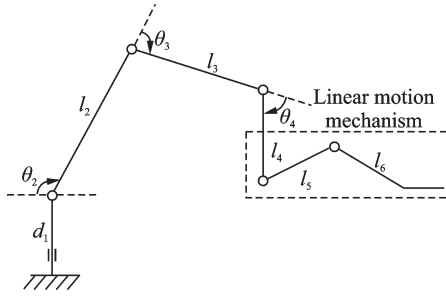


Fig.7 Schematic diagram of simplified robot mechanism and parameters

The workspace of the robot is related to the upper arm length  $l_2$ , the elbow length  $l_3$ , the vertical rod length  $l_4$ , the height  $d_1$  from the turning center to the ground, and the pitch angle  $\theta_2$  of the upper arm and the pitch angle  $\theta_3$  of the elbow. The maximum workspace of the robot is also related to the

$$\begin{cases} d_1 + l_2 \sin(180^\circ - \theta_{2\max}) - l_3 \sin[\theta_{3\max} - (180^\circ - \theta_{2\max})] - l_4 \leq 850 \\ d_1 + l_2 \sin(180^\circ - \theta_{2\max}) + l_3 \cos \theta_{3\min} - l_4 = 2800 \end{cases} \quad (20)$$

After the clamp is close to the heating furnace, the material clamping is completed by the linear motion mechanism. Considering the wall thickness of the heating furnace and the position of the material in the furnace, the rod size of the linear motion mechanism meets the requirements

$$2l_5 = l_4 \geq 1000 \quad (21)$$

#### 4.1.2 Workspace constraints

When the pitch angle of the robot's upper arm and elbow reaches the maximum and the linear mo-

$$\begin{cases} c_1(X) = x_1 + x_2 \sin \theta_{2\max} + x_3 \sin(\theta_{2\max} + \theta_{3\max}) - x_4 - 850 \leq 0 \\ c_2(X) = 1000 - x_4 \leq 0 \\ c_3(X) = 4300 + x_2 \cos \theta_{2\max} - x_3 - x_4 \leq 0 \\ \text{ceq}(X) = x_1 + 0.5x_2 + x_3 \cos \theta_{3\min} - x_4 - 2800 = 0 \end{cases} \quad (23)$$

According to the above constraints, the primary rods sizes are  $d_1 = 900$  mm,  $l_2 = 1500$  mm,  $l_3 = 2200$  mm,  $l_4 = 2l_5 = 1200$  mm.

rod length  $l_5$ . In order to reduce the total length of the rods to save material, setting  $l_4 = 2l_5$ . Taking into account the interference between the rods and the limitation of the height of the base,  $60^\circ \leq \theta_2 \leq 150^\circ$ , and  $30^\circ \leq \theta_3 \leq 135^\circ$  are determined. Then  $d_1$ ,  $l_2$ ,  $l_3$ , and  $l_5$  are determined to be the design variables, which can be expressed as

$$\begin{aligned} \mathbf{x} &= [x(1) \ x(2) \ x(3) \ x(4)] = \\ & [d_1 \ l_2 \ l_3 \ l_5] \end{aligned} \quad (19)$$

In order to make the robot meet the requirements of the material transfer operation and avoid the interference and collision between the robot rods and between the rods and the ground, the restriction conditions of the rod size include rod length restriction and workspace restriction.

#### 4.1.1 Constraint conditions of rod lengths

Considering the height of the furnace door of the heating furnace, the height of the die cavity of the die forging press and the height of the workshop, the design height of the clamp center is between 850—2800 mm. Therefore, the constraints are as follows

tion mechanism is fully deployed, the end of the robot can reach the farthest horizontal point. Combined with the requirements of the horizontal travel parameters of the transfer robot, in order to make the maximum stretch distance of the clamp of the robot not less than 4200 mm, the constraints can be obtained by

$$l_2 \cos(180^\circ - \theta_{2\max}) + l_3 + 2l_5 \geq 4200 \quad (22)$$

Converting Eq.(20) to Eq.(22) into nonlinear constraint functions, we can obtain

### 4.2 Objective function determination

The performance indexes used for kinematic size optimization are the condition number of the Ja-

cobian matrix and operability<sup>[17]</sup>, isotropy, static stiffness, the smallest or the largest singular value, etc. The condition number of the Jacobian matrix directly determines the mapping accuracy of joint space velocity to operating space velocity. The number also reflects the degree of distortion of the transfer relationship between the joint input velocity and the end-effector output velocity. The minimum value of the Jacobian matrix condition number is 1. When the Jacobian condition number of the robot is 1 in its working space, the corresponding configuration is kinematic isotropic, and the transmission performance of the mechanism is the best. The larger the Jacobian condition number is, the larger deviation of the end manipulator's velocity caused by the deviation of the input angular velocity. At the same time, the distortion of the transfer relationship between the motion input and the output is more serious when solving the inverse solution of the joint angular velocity. Therefore, the Jacobian matrix condition number  $k$  is used as an evaluation index of robot motion performance.

From the definition of the matrix condition number, the relationship  $k$  with the Jacobian matrix  $J$  is

$$k = \|J\| \cdot \|J^{-1}\| \quad (24)$$

where  $\|J\|$  is the norm of the Jacobian matrix  $J$ , and  $\|J^{-1}\|$  the norm of the Jacobian inverse matrix.

The common norms for any matrix are 1 norm  $\|A\|_1 = \max_{1 \leq j \leq n} \sum_{i=1}^n |a_{ij}|$ ,  $\infty$  norm  $\|A\|_\infty = \max_{1 \leq i \leq n} \sum_{j=1}^n |a_{ij}|$ , 2 norm  $\|A\|_2 = \sqrt{\rho(A^H A)}$  and F norm  $\|A\|_F = \sqrt{\text{tr}(A^H A)}$ . Among them,  $\rho(A^H A) = \max_{1 \leq i \leq n} |\lambda_i|$  is

$$J^{-1} = \begin{bmatrix} 0 & 0 & 0 & 1 \\ \frac{s_4}{l_2 c_1 c_{24}} & \frac{c_4}{l_2 c_{24}} & -\frac{2l_5 s_4 c_5}{l_2 c_1 c_{24}} & \frac{s_1 s_4 (l_2 c_2 - l_3 s_4 + 2l_5 s_5)}{l_2 c_1 c_{24}} \\ -\frac{c_2}{l_3 c_1 c_{24}} & -\frac{s_2}{l_3 c_{24}} & \frac{2l_5 c_2 c_5}{l_3 c_1 c_{24}} & -\frac{s_1 c_2 (l_2 c_2 - l_3 s_4 + 2l_5 s_5)}{l_3 c_1 c_{24}} \\ 0 & 0 & \frac{1}{c_1} & 0 \end{bmatrix} \quad (28)$$

From Eq.(25), the Jacobian condition number  $k$  is

the spectral radius of  $A^H A$ ,  $\lambda_i$  is the eigenvalue of  $A^H A$ ,  $\text{tr}(A^H A)$  is the trace of  $A^H A$ ,  $A^H$  is the transposed matrix of  $A$ .  $k$  depends on the choice of matrix norm, and satisfies  $1 \leq k \leq \infty$ .

Since 1 norm,  $\infty$  norm and 2 norm change with the joint angle  $\theta_i$  and the rod length  $l_i$ , the size judgment must be carried out first in the calculation process. Therefore, the condition number of the Jacobian matrix is defined by the F norm

$$k = \|J\|_F \cdot \|J^{-1}\|_F = \sqrt{\text{tr}(J^H J)} \sqrt{\text{tr}((J^{-1})^H (J^{-1}))} \quad (25)$$

Because the Jacobian matrix of the robot is determined by its configuration, different joint angles correspond to different Jacobian matrices. Therefore, the Jacobian condition number is a local performance index. Gosselin proposed a velocity global performance index  $\eta$  to represent the average value of the Jacobian condition number in the workspace, which can be expressed as

$$\eta = \frac{\int_R k d\theta_n \cdots d\theta_2 d\theta_1}{\int_R d\theta_n \cdots d\theta_2 d\theta_1} \quad (26)$$

The range of  $\eta$  is  $[1, \infty)$ . The smaller  $\eta$  is, the better global performance of the robot velocity is. Taking minimum of  $\eta$  as the optimization objective, the objective function can be given as

$$F(x) = \min(\eta) \quad (27)$$

## 5 Size Optimization Results and Workspace Analysis

From Eq.(18), the inverse matrix of the Jacobian matrix of the heavy-load robot is

$$k = \sqrt{\sum_{i=1}^4 \sum_{j=1}^4 (a_{ij})^2} \sqrt{\sum_{i=1}^4 \sum_{j=1}^4 (b_{ij})^2} \quad (29)$$

From Table 1 and Eq.(2),  $\theta_4 \in [-15^\circ, 165^\circ]$ . According to Eq.(26), the global performance index of velocity  $\eta$  is the function of length  $l_i$  of member, which satisfies

$$\eta = \frac{\int_{-\pi}^{\pi} \int_{\frac{\pi}{3}}^{\frac{5\pi}{6}} \int_{\frac{\pi}{4}}^{\frac{3\pi}{4}} \int_{-\frac{\pi}{2}}^{\frac{\pi}{2}} kd\theta_5 d\theta_4 d\theta_2 d\theta_1}{\int_{-\pi}^{\pi} \int_{\frac{\pi}{3}}^{\frac{5\pi}{6}} \int_{\frac{\pi}{4}}^{\frac{3\pi}{4}} \int_{-\frac{\pi}{2}}^{\frac{\pi}{2}} d\theta_5 d\theta_4 d\theta_2 d\theta_1} = \eta(l_2, l_3, l_5) = \eta(x(2), x(3), x(4)) \quad (30)$$

With the initial value  $X_0 = [1\ 500, 2\ 200, 600]$  selected,  $F(x) = \min(\eta)$  as the optimization objective and Eq.(23) as the constraint condition, and the constrained minimization function `fmincon` in MATLAB optimization toolbox is called, the optimization result is obtained which is  $X = [1\ 614.23, 1\ 807.64, 501.58]$ . From Eq.(23),  $d_1 = 800$ . After optimization, the sizes of the manipulator rods are  $d_1 = 800$  mm,  $l_2 = 1\ 600$  mm,  $l_3 = 1\ 800$  mm, and  $l_4 = 2l_5 = 1\ 000$  mm. Table 3 shows the change of the global performance index of velocity  $\eta$  and the total length  $L_2 + L_3 + L_4$  of the rods before and after the size optimization. After optimization, the total length of the rods is reduced by 6.12%. The global speed performance is improved by 45.15%, and the robot has less consumables and lighter weight.

**Table 3 Comparison of optimization results**

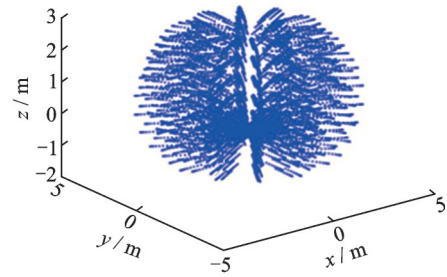
Index	$\eta$	$(L_2 + L_3 + L_4)/\text{mm}$
Before optimization	55.68	4 900
After optimization	30.54	4 400
Optimization degree/%	45.15	6.12

The robot workspace refers to the set of all space points which can be reached by the robot end manipulator under normal working conditions. From Eq.(4), the position coordinates of the end clamp of the robot are

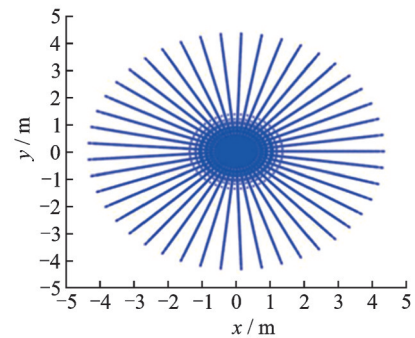
$$\begin{cases} p_x = (l_2 \cos \theta_2 - l_3 \sin \theta_4 + 2l_5 \sin \theta_5) \cos \theta_1 \\ p_y = (l_2 \cos \theta_2 - l_3 \sin \theta_4 + 2l_5 \sin \theta_5) \sin \theta_1 \\ p_z = l_2 \sin \theta_2 - l_3 \cos \theta_4 - l_4 + d_1 \end{cases} \quad (31)$$

According to the range of motion of each joint

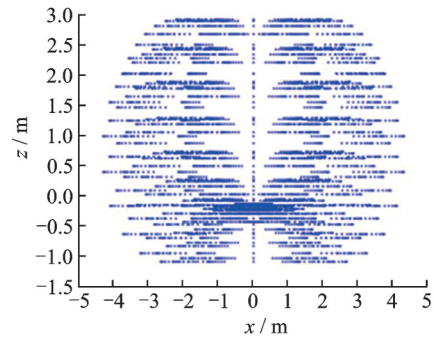
angle and the optimized rod length  $d_1 = 800$  mm,  $l_2 = 1\ 800$  mm,  $l_3 = 1\ 800$  mm,  $l_4 = 2l_5 = 1\ 000$  mm in Table 1. As shown in Fig.8, the workspace of the robot is obtained by MATLAB simulation. The results show that the robot workspace meets the space requirements of the task.



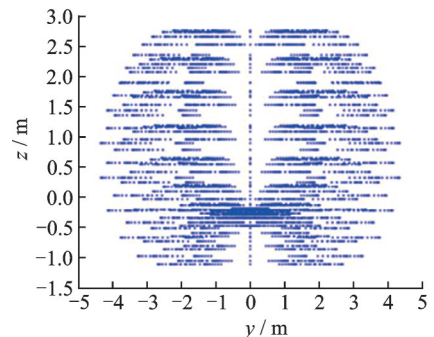
(a) Axonometric view of workspace



(b) Workspace projection in *xoy* plane



(c) Workspace projection in *xoz* plane



(d) Workspace projection in *yoz* plane

Fig.8 Workspace distributions of transfer robot

## 6 Conclusions

A configuration design scheme of a 4-DOF transport robot with multi parallel four-bar mechanisms is proposed. In order to design a robot with better velocity transmission performance in the whole workspace, the optimization of the length of the rod and the spatial analysis of the movement of the transfer robot are carried out by taking the global performance index of velocity as the optimization goal. The main conclusions are as follows:

(1) Based on the technical parameters and task requirements of the heavy-load transfer robot, a 4-DOF material transport robot with multi parallel four-bar mechanisms is designed. The structure of the robot takes the parallelogram motion chain as the main structure to improve the strength and stiffness of the robot. The Jacobian matrix of the robot is obtained by using the D-H parameter method, total differential equation method and vector product method.

(2) Taking the lengths of the main rods as design variables, the global performance index of velocity as the objective function, and the actual working condition of the robot as the constraint condition, the length of the rod is optimized by MATLAB simulation. Based on the optimized length of the rod, the workspace of the end manipulator in the global coordinate system is solved by programming. The workspace of the robot fully meets the design requirements.

### References

- [1] MENG Minghui, ZHOU Chuande, CHEN Libin, et al. A review of the research and development of industrial robots[J]. *Journal of Shanghai Jiao Tong University*, 2016, 50(S1): 98-101. (in Chinese)
- [2] LIU Fengchen, YAO Yunfeng, LIU Liming, et al. Development and application of high-speed transfer robots industry[J]. *Light Industry Machinery*, 2012, 30(2): 108-112. (in Chinese)
- [3] SUN Wei, ZHANG Yongxing, ZHAO Yongjie, et al. Research status of heavy-duty industrial robots[J]. *Journal of Shantou University (Natural Science)*, 2020, 35(1): 3-15. (in Chinese)
- [4] YANG S Y, KIM Y G, RYOO Y J, et al. Simulation of design conditions of logistics robot transferring heavy load[C]//*Proceedings of 2017 14th International Conference on Ubiquitous Robots and Ambient Intelligence (URAI)*. [S.l.]: IEEE, 2017: 322-324.
- [5] FUKUI R, YAMADA Y, MITSUDOME K, et al. HanGrawler: Large-payload and high-speed ceiling mobile robot using crawler[J]. *IEEE Transactions on Robotics*, 2020, 36(4): 1053-1066.
- [6] ZHU Jianwen, ZHOU Bo, MENG Zhengda. Kinematic analysis and simulation of 150 kg robot based on Adams[J]. *Industrial Control Computer*, 2017, 30(7): 82-84, 87. (in Chinese)
- [7] MA L, BI D X, XIAO Z P. Mechanism simulation and experiment of 3-DOF parallel robot based on MATLAB[C]//*Proceedings of 2015 International Power, Electronics and Materials Engineering Conference*. Dalian, China: Atlantis Press, 2015.
- [8] RIOUX A, SULEIMAN W. Autonomous SLAM based humanoid navigation in a cluttered environment while transporting a heavy load[J]. *Robotics and Autonomous Systems*, 2018, 99: 50-62.
- [9] YANG Qianming, RUAN Yi, ZHANG Jun. Dynamics simulation and analysis of heavy-load handling compound robot based on ADAMS[J]. *The Journal of New Industrialization*, 2018, 8(3): 34-39. (in Chinese)
- [10] WANG Xuelei, ZHANG Bin, LI Chuanjun, et al. Analysis for global performance index of 5UPS-RPS parallel mechanism based on Jacobian matrix[J]. *Transactions of Beijing Institute of Technology*, 2018, 38(9): 899-904. (in Chinese)
- [11] XIONG Yanmei, YANG Yandong. Kinematics simulation of palletizing robot[J]. *Machinery*, 2015, 42(1): 62-66. (in Chinese)
- [12] HAWLEY L, SULEIMAN W. Control strategy and implementation for a humanoid robot pushing a heavy load on a rolling cart[C]//*Proceedings of 2017 IEEE/RSJ International Conference on Intelligent Robots and Systems (IROS)*. [S.l.]: IEEE, 2017: 4997-5002.
- [13] LIU He, WAN Jun, ZENG Hui, et al. Kinematics analysis and research for functions of palletizing robot with double parallelogram[J]. *Machine Tool & Hydraulics*, 2015, 43(23): 62-64. (in Chinese)
- [14] WEI Yajun, QIU Guoliang, DING Guanghe, et al. A structural optimization design method for heavy-duty

- palletizing robot[J]. Chinese Journal of Engineering Design, 2020, 27(3): 332-339. (in Chinese)
- [15] PAN S L, WANG C. Literature review of RV reducer test bed[J]. IOP Conference Series: Materials Science and Engineering, 2019, 542: 71-88.
- [16] CHENG H, JIA R X, LI D D, et al. The rise of robots in China[J]. Journal of Economic Perspectives, 2019, 33(2): 71-88.
- [17] CHEN Qiyu, WU Zhiheng. Comparative analysis on development strategies of worldwide industrial robot industries[J]. Automation & Information Engineering, 2017, 38(2): 1-6. (in Chinese)
- [18] HAN Xiushu, WANG Jidai, WEI Junying, et al. Kinematics analysis of palletizing robot[J]. Journal of Mechanical Transmission, 2014, 38(9): 109-112. (in Chinese)
- [19] YAN Chengxin. Study on Jacobian matrices of the large scale shotcrete-robot[J]. Modular Machine Tool & Automatic Manufacturing Technique, 2010(7): 5-7, 11. (in Chinese)

**Acknowledgements** This work was supported by the Na-

tional Key R&D Program of China (No.2018YFB1307900), the Natural Science Foundation of Shanxi Province (Nos. 201901D211009, 201901D211010) and the Technology Innovation Foundation of Shanxi University (No. 2019L0177).

**Author** Dr. ZHANG Jing received the M.S. degree in mechatronic engineering from Dalian University of Technology in 2009 and Ph.D. degree in manufacturing engineering of aerospace vehicle from Harbin Institute of Technology in 2014, respectively. Her research is focused on mechanism.

**Author contributions** Dr. ZHANG Jing proposed the design method, planned the research contents, and wrote the manuscript. Mr. WANG Dongbao and Mr. WU Guangping contributed to the analysis of the model. Prof. GUO Hongwei and Prof. LIU Rongqiang contributed to the discussion and background of the study. All authors commented on the manuscript draft and approved the submission.

**Competing interests** The authors declare no competing interests.

(Production Editor: WANG Jing)

## 平行四连杆式重载转运机器人机构设计与运动分析

张 静<sup>1</sup>, 王东宝<sup>1</sup>, 武广平<sup>2</sup>, 郭宏伟<sup>3</sup>, 刘荣强<sup>3</sup>

(1. 太原理工大学机械与运载工程学院, 太原 030024, 中国; 2. 上海交通大学电子信息与电气工程学院, 上海 200240, 中国; 3. 哈尔滨工业大学机器人技术及系统国家重点实验室, 哈尔滨 150001, 中国)

**摘要:** 重载转运机器人被广泛用于汽车生产和机械制造等行业, 可显著提高生产效率。为满足大型坯料转运需求, 本文提出一种平行四连杆式四自由度转运机器人构型设计方案。雅可比矩阵是指从关节速度到转移机器人操作空间速度的映射矩阵, 可以用微分矢量法求解。将雅可比矩阵条件数在工作空间内的均值作为机器人速度全域性能指标, 并以速度全域性能指标为优化目标。然后, 以机器人实际工况为约束条件, 开展杆件长度优化, 并获得最小的杆件总长度和全域速度性能指标数, 优化前后, 机器人杆件长度总和减少 6.12%, 全域速度性能提升 45.15%。以优化后的杆件尺寸作为机构参数, 通过仿真分析获得转运机器人的运动空间分布。最后, 结果表明, 所提的少自由度雅可比矩阵建立方法和基于速度全域性能指标的杆件优化准确、有效, 机器人的工作空间分布满足设计要求。

**关键词:** 参数优化; 运动分析; 机构设计; 转运机器人; 重载